Doubly Reentrant Cavities Prevent Catastrophic Wetting Transitions on Intrinsically Wetting Surfaces

ACS APPLIED MATERIALS & INTERFACES

Article

Doubly Reentrant Cavities Prevent Catastrophic Wetting Transitions on Intrinsically Wetting Surfaces

Eddy Domingues, Sankara Arunachalam, and Himanshu Mishra

ACS Appl. Mater. Interfaces, **Just Accepted Manuscript** • DOI: 10.1021/acsami.7b03526 • Publication Date (Web): 05 Jun 2017

ACS Publications

ACS Applied Materials & Interfaces is published by the American Chemical Society. 1155 Sixteenth Street N.W., Washington, DC 20036

Doubly Reentrant Cavities Prevent Catastrophic Wetting Transitions on Intrinsically Wetting Surfaces

*Eddy M. Domingues,‡ Sankara Arunachalam,‡ Himanshu Mishra**

E. M. Domingues, S. Arunachalam, H. Mishra

King Abdullah University of Science and Technology (KAUST), Water Desalination and Reuse Center (WDRC), and Biological and Environmental Science and Engineering (BESE) Division, Thuwal 23955-6900, Saudi Arabia

KEYWORDS

Doubly reentrant cavities, omniphobicity, damage-tolerance, underwater hydrophobicity, wetting transitions, immersion in mineral oil, vapor pressure, capillary bridges

ABSTRACT

Omniphobic surfaces, i.e. which repel all known liquids, have proven of value in applications ranging from membrane distillation to underwater drag reduction. A limitation of currently employed omniphobic surfaces is that they rely on perfluorinated coatings, increasing cost and environmental impact, and preventing applications in harsh environments. There is, thus, a keen interest in rendering conventional materials, such as plastics, omniphobic by micro/nano-texturing rather than via chemical make-up, with notable success having been achieved for silica surfaces with doubly reentrant micropillars. However, we found a critical limitation of microtextures comprising of pillars that they undergo catastrophic wetting transitions (apparent contact angles, $\theta_r \rightarrow 0°$ from $\theta_r > 90°$) in the presence of localized physical damages/defects or on immersion in wetting liquids. In response, a doubly reentrant cavity microtexture is introduced, which can prevent catastrophic wetting transitions in the presence of localized structural damage/defects or on immersion in wetting liquids. Remarkably, our silica surfaces with doubly reentrant cavities could exhibited apparent contact angles, $\theta_r \approx 135°$ for mineral oil, where the intrinsic contact angle, $\theta_o \approx 20°$. Further, when immersed in mineral oil or water, doubly reentrant microtextures in silica ($\theta_o \approx 40°$ for water) were not penetrated even after several days of investigation. Thus, microtextures comprising of doubly reentrant cavities might enable applications of conventional materials without chemical modifications, especially in scenarios that are prone to localized damages or immersion in wetting liquids, e.g. hydrodynamic drag reduction and membrane distillation.

INTRODUCTION

Natural and human-made surfaces are termed as omniphobic if they have a tendency to *repel* all liquids; droplets of liquids placed on omniphobic surfaces exhibit apparent contact angles, $\theta_r > 90°$. Omniphobic surfaces are employed in numerous applications including self-cleaning mirrors and windshields,[1-2] anti-icing coatings,[3] membrane distillation,[4-5] membrane vapor extraction,[6] oil-water separation,[7-8] and reduction of hydrodynamic drag[9-13] and biofouling[14]. Typically, omniphobicity is achieved by stabilizing/trapping air between the liquid and the solid surface (also known as Cassie-states or partially-filled states)[15] and preventing wetting transitions to the fully-filled (Wenzel state)[16]. A limitation of current omniphobic surfaces, however, is their reliance on perfluorinated chemicals,[1-4, 7-9, 14, 17-23] which restricts their usage due to degradation under harsh physical and chemical conditions,[24-26] cost, and environmental and health concerns.[27-28] Thus, there exists a need for alternative strategies to render conventional materials, such as polyethyleneterepthalate (PET), aluminum, and low-carbon steels, omniphobic without using perfluorinated compounds. In this direction, theoreticians and experimentalists have proposed several surface topographies comprising of overhanging (reentrant) features, mostly pillars, which could trap air and prevent penetration of liquids.[29-37] Most recently, inspired by the skin of Springtails (*Collembola*),[34, 38-39] Liu and Kim microfabricated arrays of doubly reentrant pillars on silicon wafers that exhibited still greater omniphobicity, now termed superomniphobicity, defined by apparent contact angles $\theta_r > 150°$ and extremely low contact angle hysteresis for a variety of polar and non-polar liquids (though, some non-polar liquids, such as FC-40 and FC-70, imbibed into the microtexture over time via capillary condensation).[40-41] We consider this approach to be crucial in creating next-generation applications of omniphobic surfaces from conventional materials.

Interestingly, in our investigation, we found that intrinsically wetting surfaces with micropillars—simple, reentrant, and doubly reentrant—suffer from catastrophic wetting transitions in the presence of localized physical damage/defects or on immersion in wetting liquids (more weaknesses were recently listed by Werner and co-workers[37]). We provide a demonstration of catastrophic wetting transitions in the presence of localized damage/defects and immersion in wetting liquids by placing a drop of water at the edge of a silica surface with doubly reentrant micropillars (Figure 1A, Figure S1 and Movie S1 in SI). Interestingly, the sites of localized physical damage/defects could act as wicks for wetting liquids. The Laplace pressure of the invading liquid menisci, $P_L = \gamma_{LV}(1/r_1 + 1/r_2)$, expels the air trapped within the micropillar texture, where γ_{LV} is the surface tension of the liquid and r_1 and r_2 are the orthogonal radii of curvature of the liquid-vapor interface (Figure 1A).[42] As a result of these catastrophic wetting transitions, apparent contact angles could reduce instantaneously from $\theta_r \geq 150°$ to $\theta_r \rightarrow 0°$, which would impact potential applications. Thus, we submit that all known pillar-based microstructures might be unsuitable for applications that risk localized physical damage or immersion in wetting liquids. In response to these serious limitations, we considered microfabricating surfaces with doubly reentrant cavities - we foresaw that doubly reentrant edges of cavities would stabilize Cassie-states and the compartmentalized nature of cavities would prevent the spread of catastrophic wetting transitions from localized damages/defects (Figure 1B).

RESULTS AND DISCUSSION

We microfabricated doubly reentrant cavities (Figure 2) on silicon wafers with a 2.4 µm thick thermally grown silica layer by adapting the method reported by Liu et al. (Details in

Experimental Section).[40] In order to minimize the real liquid-solid contact area (A_{LS}) and maximize the liquid-vapor contact area (A_{LV}), we chose arrays of square cavities with rounded corners (corner radius r = 3 μm). The cavity edge length, D, ranged from 100-250 μm, with depth h ≈ 50 μm, and pitch (i.e. the center-to-center distance between adjacent cavities) $L = D +$ 12 μm (Figure 2 and Figure S2 in SI). To investigate the influence of the size of the doubly reentrant overhang, w, on wetting, we also microfabricated arrays with a smaller pitch, $L = D + 5$ μm (Figure S3 in the SI). Unfortunately, doubly reentrant cavities with smaller pitch ($L = D + 5$ μm) exhibited poorer surface finish due to the resolution limit of our photolithographic techniques, so we focused on samples with larger pitch ($L = D + 12$ μm). Table S1 in the SI presents a summary of various doubly reentrant cavities and pillars that were investigated for this study.

Flat silica surfaces are intrinsically wetting (intrinsic contact angle, $\theta_o < 90°$) to most polar and nonpolar liquids. We chose water as the polar liquid for investigating wetting of our surfaces because of its ubiquity and ease of usage (surface tension, γ_{LV} = 72 mN m^{-1} and equilibrium partial pressure, p_W = 2.3 kPa at NTP, and $\theta_o \approx 40°$). We chose mineral oil as a representative non-polar liquid due to its low vapor pressure (γ_{LV} = 30 mN m^{-1} and p_W < 10 Pa at NTP, and $\theta_o \approx 20°$, more details in the Experimental Section). A detailed report on the behavior of high vapor pressure wetting liquids, such as ethanol, where consideration of capillary condensation and evaporation is crucial, will be communicated shortly. We observed apparent contact angles, $\theta_r > 120°$ for typical sessile drops of volume, $V \approx 2$ μL, for both mineral oil and water (Figure 3, Table S1 and Section Si in the SI). Since the characteristic sizes of the sessile drops were lower than their capillary lengths, and the volume of the air-filled cavities underneath the drops was much lower than volumes of drops, we could apply the Cassie-Baxter model to predict apparent contact angles and found a reasonable agreement (Figure 3, Sections S1 and S2 in the SI).[15, 42]

Interestingly, we found that contact angle hysteresis of wetting liquids on doubly reentrant silica cavities was significantly larger than for doubly reentrant pillars (Figure 3). As a consequence, drops of water (or mineral oil) did not bounce off from the surface of doubly reentrant cavities. We consider that in the case of pillars, the receding liquid meniscus detaches periodically from disconnected pillars, whereas for cavities, connected wetting pathways pervade, which promote pinning and low receding contact angles (θ_R).[43-45] Fascinatingly, when we observed receding water menisci on our doubly reentrant silica cavities via upright optical microscopy, we noticed suspended films of water (hereafter referred to as 'capillary bridges') left behind at the mouths of the cavities (Figure 5 and Movie S2 in the SI). Subsequently, due to evaporation, capillary bridges thinned out and broke, leading to fine microdroplets, some of which can be seen in Figure 5(F). We could not investigate evolution of capillary bridges in the case of mineral oil because they did not evaporate under our experimental conditions. While the time- and speed-dependent dynamics of formation/breaking of these capillary bridges is beyond the scope of this work, we consider them to contribute to contact angle hysteresis.[46] We speculate that a hierarchical structure comprising of nanoscale doubly reentrant pillars onto doubly reentrant cavities might present a solution (Section S3 in the SI). For completeness, we also investigated effects of coating our microtextured silica surfaces with perfluorodecyltrichlorosilane (FDTS) on the contact angle hysteresis with water and mineral oil (Details in the Experimental Section). Whereas drops of water falling from a height of 6 mm on our FDTS-coated samples bounced off indicating low contact angle hysteresis (Movie S3, SI), mineral oil drops did not (Figure S4 in the SI, displays intrinsic, advancing and receding contact angles for both the liquids).

As demonstrated above, silica surfaces with doubly reentrant pillars underwent catastrophic wetting transitions if a wetting liquid, such as water or mineral oil, was placed at the edge of the microtexture (Movie S1 in SI), or if the surface was immersed in a wetting liquid. In fact, all intrinsically wetting surfaces with pillar geometries—doubly reentrant, reentrant, or non-reentrant—would exhibit this behavior (Figure 1A). In contrast, on silica surfaces with doubly reentrant cavities, we found that there were no catastrophic wetting transitions if water or mineral oil was placed on the edges (Movie S4 in SI and Figure 1B), or if surfaces were immersed in wetting liquids, or if there were localized physical damages/defects (Figure 4).

Next we investigated time-dependence of wetting of doubly reentrant cavities on silica surfaces immersed in water and mineral oil (Figure 4 and Figure S5 in the SI). For consistency, all the microtextured silica samples were cleaned with piranha solution and stored in sealed polystyrene petri dishes in a clean nitrogen flow cabinet for two weeks (Details in the Experimental Section). As a result, the intrinsic contact angle of water on smooth silica stabilized from $\theta_o \approx 0°$ to $\theta_o \approx 40°$, which is indicative of partial dehydration of the surface and unavoidable adsorption/desorption of airborne contaminants in equilibrium with the local environment.[47-49] Thus, we consider our surfaces to be representative of common wetting surfaces in the real world. We placed our silica surfaces with doubly reentrant cavities under a ~5 mm column of deionized water (hydrostatic pressure, $P_H = \rho g h = 49\ Pa$) and observed from the top using an Edmund USB3 monochrome camera at a speed of 2 frames/sec (Figure 4). Since light reflected by a flat air-water interface is markedly different from light reflected by bulged menisci, we could differentiate between them (Figure 4A and 4G, respectively). We found that the intruding liquid menisci assumed a flat profile for the first 4 hours, followed by upward bulging. We hypothesized that this bulging was due to appearance of water in the cavities, via capillary condensation[50] and liquid imbibition along the corners,[51-54] which displaced the trapped air, that could not rapidly dissolve in the water (Henry's constant for air in water, H_{air} =1161 atm L mol $^{-1}$ at NTP[55]) (Figure 4E-G). This upward bulging continued for about two weeks after which it slowed down and decreased, driven by dissolution of air in water (Figure 4G-I). To test our claim that the doubly reentrant cavities would prevent catastrophic wetting transitions in the presence of localized physical damage/defects, we included cavities that were interconnected, i.e. damaged, during the microfabrication process, in the immersion experiment. Here we indicate specific cavities by (Column#, Row#) in the snapshots at various times to explain our observations. We observed that water readily penetrated into the interconnected cavities (# [1,3], [1,4] and [2,3]) and a portion of trapped gas was released as a bubble. A smaller bubble was left behind, which dissolved over time (cavity # [2,3] in Figure 4A-F). However, the surrounding cavities remained undisturbed. In a nutshell, we found that 90% of the water-wet silica cavities stored underwater did not get filled even after 30 days. We also performed immersion experiments with mineral oil and found that menisci stabilized at the doubly reentrant edges followed by downward bulging, most probably because of the dissolution of gases in mineral oil (Figure S5 in the SI). Further investigation on wetting transitions of mineral oil in doubly reentrant silica microtextures via complementary experimental techniques is underway.

To investigate pressure-dependence of wetting transitions, we subjected our silica surfaces with doubly reentrant cavities (D = 200 μm, $L = D$ + 12 μm) to elevated pressures in a home-built pressure cell (Figures S6 and S7 in the SI). We found that water menisci remained stable at the edges of doubly reentrant cavities in the majority of cavities, up until an additional pressure of 103.1 kPa (Figure S6 A-C, in the SI), beyond which, water penetrated (Figure S6 D, in the SI). We consider that some cavities failed quicker than others due to inhomogeneity in our microfabrication process as mentioned earlier. Interestingly, under enhanced pressure, trapped air dissolved faster and wetting transitions towards the fully-filled state were found to be quicker.

Even though catastrophically wetting transitions are prevented even in the presence of localized physical damage/defects on doubly reentrant cavity microtextures, we know that at the thermodynamic equilibrium wetting liquids will completely fill the cavities.[56-61] However, the kinetics of wetting transitions could be tuned via intrinsic contact angles, shapes and sizes of cavities (including doubly reentrant edges and corner radii), rates of capillary condensation and imbibition through corners, and the solubility of the trapped gas in the liquid.[36, 50, 52-54, 62-68] For example, we note dramatically different behaviors of water versus mineral oil on our freshly cleaned surfaces (with piranha solution or oxygen plasma; details in the Experimental Section). We found that upon immersion in water ($\theta_o \approx 0°$), our square-shaped doubly reentrant cavities got instantaneously filled with concomitant release of air bubbles (Movie S5 in the SI). In contrast, upon immersion in mineral oil ($\theta_o \approx 20°$) the liquid menisci were stabilized in a Cassie-states, similar to as shown in Figure S5(A) in the SI. This observation points to the crucial role of intrinsic contact angles and capillary condensation on wetting transitions; detailed investigations are warranted.

We would like to clarify that doubly reentrant cavities could prevent catastrophic wetting transitions in the presence of localized surface damage/defects only, but not under uniform surface damage, such as incurred during a Crockmeter test. While our silica microtextures are quite fragile, our expectation is that this proof-of-concept could be translated to commonly available robust materials via inexpensive methods, such as injection molding.[69] Having said that, we do note that for similar area fractions of liquid-solid and solid-vapor contacts, microtextures with cavities might exhibit higher mechanical strength against mechanical stresses than pillars.[37]

CONCLUSIONS

We demonstrated that omniphobicity of intrinsically wetting surfaces adorned with pillar-based microtextures was vulnerable to localized physical damages/defects and immersion in wetting liquids. In response, we introduced doubly reentrant cavities that exhibited Cassie-states on exposure to wetting liquids by stabilizing intruding liquid menisci and trapping air underneath. Remarkably, due to the compartmentalized nature of this microtexture, catastrophic wetting transitions could be prevented even in the presence of localized surface damage/defects or immersion in wetting liquids, including water and mineral oil. While the apparent contact angles of water and mineral oil on our silica surfaces with doubly reentrant cavities were $\theta_r > 120°$, contact angle hysteresis was quite high. We consider that formation of capillary bridges at the mouths of cavities left behind receding liquid meniscus might be responsible for this behavior. We anticipate that insights from this work might advance the development of robust omniphobic surfaces exploiting common materials without further chemical modification, especially for applications that are prone to localized damages or immersion in wetting liquids. For further insights into the dependence of wetting transition mechanisms on intrinsic contact angles, shapes of cavities, and capillary condensation concerted experimental and theoretical investigations are needed.

FIGURES

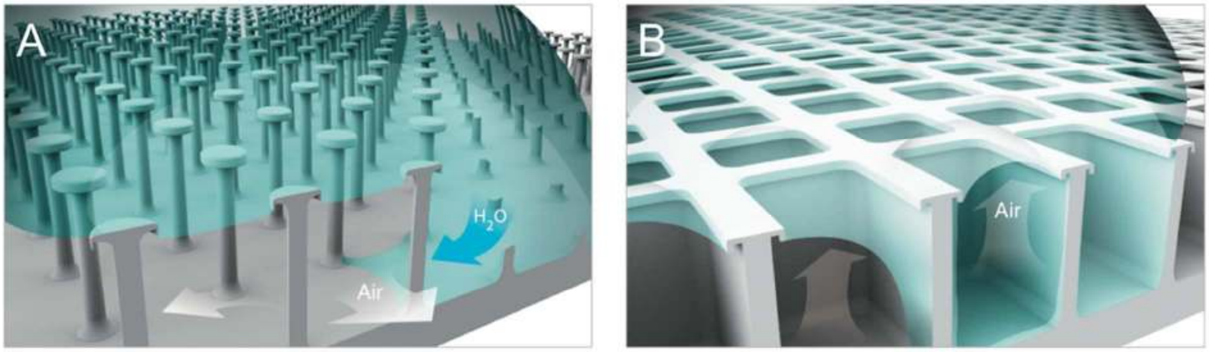

Figure 1. (A) An isometric schematic representation of a liquid drop on an array of doubly reentrant pillars with a discontinuity induced by physical damage (shown as broken pillars to the right side of the image) – Liquid imbibes laterally inward pushing out the gases underneath. (B) An isometric schematic representation of doubly reentrant cavities, which trap air inside them and physical damages are localized. (Note: in both schematics, the solid surface is liquid-wet, i.e. intrinsic contact angle, $\theta_o < 90°$)

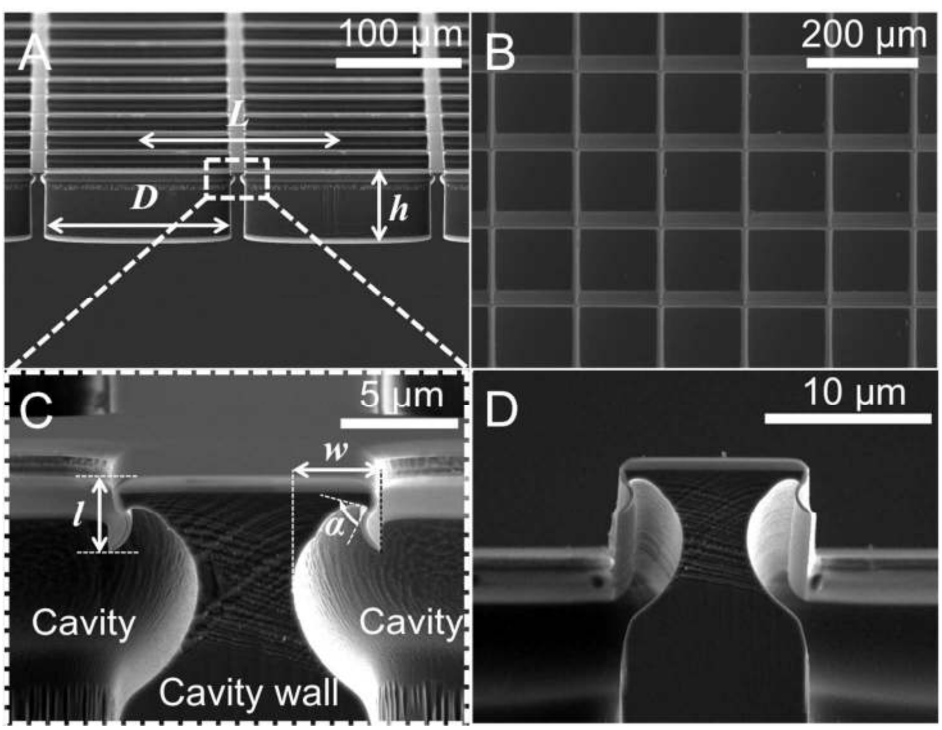

Figure 2. Representative SEM micrographs of silica surfaces with a square distribution of doubly reentrant cavities (D = 150 μm and pitch $L = D + 12$ μm) (A) Tilted (5°) cross-section view of an array; (B) Tilted (5°) top view of an array; (C) Tilted (5°) cross-section showing detail of a doubly reentrant edge; (D) Tilted (-5°) cross-section detail showing the underside of a doubly reentrant edge. D - length of the cavity, L - pitch of the cavities array of distribution where $L - D$ represents the thickness of walls, w - extent of the doubly reentrant edge, l - depth of the doubly reentrant edge, and α - angle the edge makes with the cavity wall.

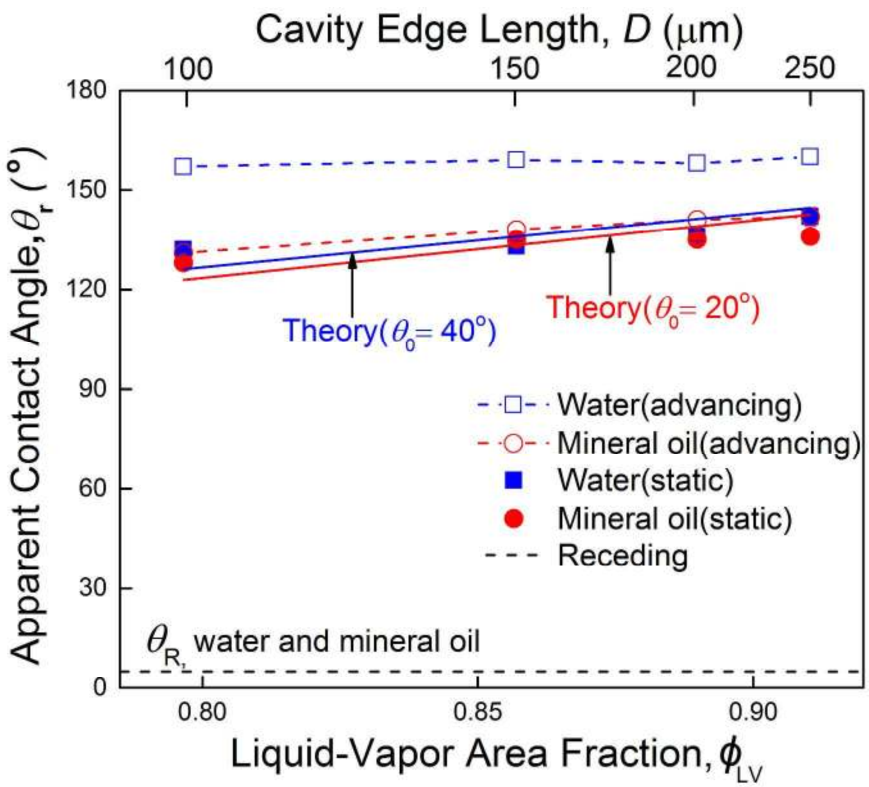

Figure 3. Static (full symbols) and advancing/receding (hollow symbols) contact angles for water and mineral oil on silica surfaces with doubly reentrant cavities (pitch, $L = D + 12$ μm) as a function of liquid-vapor area fraction, ϕ_{LV} (More details are provided in Table S1 in SI). Dotted lines were added to facilitate visualization. Solid lines show theoretical fits of the equilibrium apparent contact angles obtained from the Cassie-Baxter model ($\theta_o \approx$ 40° for water and $\theta_o \approx$ 20°

for mineral oil, both on silica). The receding contact angles for water and mineral oil were smaller than 5°.

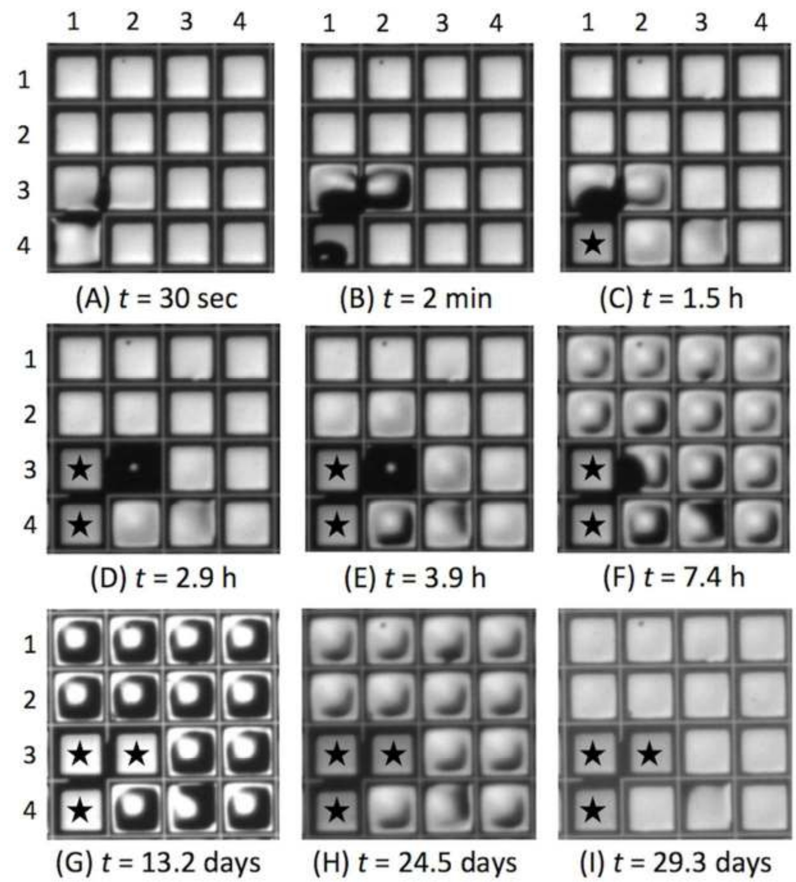

Figure 4. Optical micrographs (top view) of an array of doubly reentrant cavities on a silica surface immersed underwater (similar behavior was observed for immersion in mineral oil). The cavities filled with water are marked with a star (□) shape, all other remained unfilled for the duration of the experiment. (A-G) cavities (1,3), (1,4) and (2,3) were interconnected due to a localized physical damage. In these cavities, wetting transitions to the fully-filled state was observed in 3 hours. Remarkably, cavities adjacent to the damaged ones were unaffected and liquid menisci remained stabilized at doubly reentrant edges. (G-I) Over time, water menisci bulged upwards, probably due to capillary condensation of water and concominatnt displacement

of trapped air, followed by a gradual reduction in bulging, perhaps due to dissolution of trapped air in water, and did not get filled by water during the duration of the experiment. (Scale bar: the length of cavities is 250 μm)

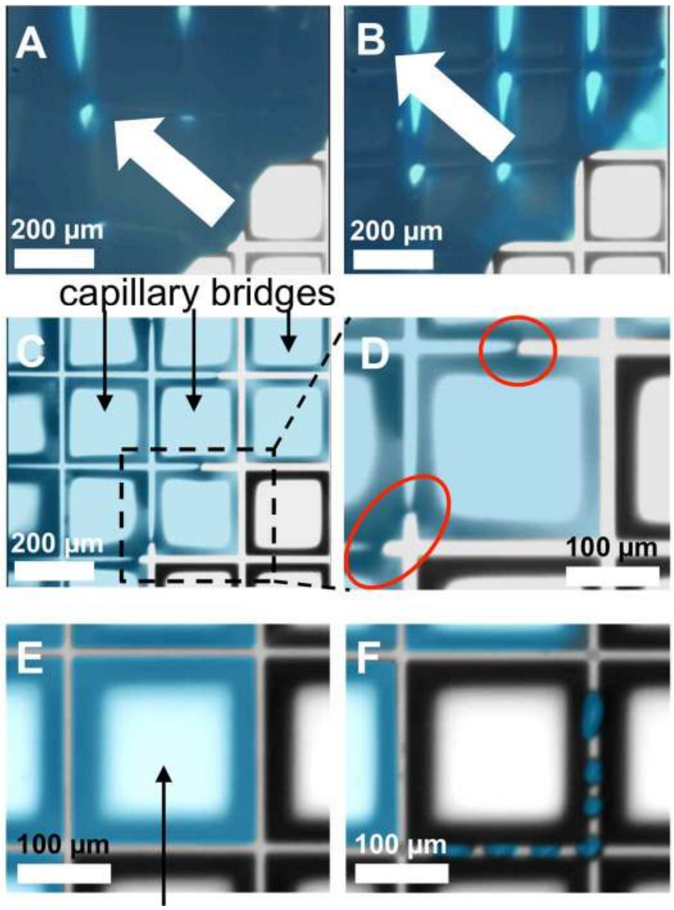

Figure 5. Representative optical micrographs (top-view) of receding water drops on a silica surface with square-shaped doubly reentrant cavities with rounded corners (false-color has been added to water to aid visualization). (A) A region at the periphery of a water droplet just before receding. In this state, the liquid drop is stabilized at the doubly reentrant edges of the microtexture. (B) As the droplet recedes, intrinsically wetting silica microtexture pins water. (C) As a result, the receding meniscus leaves behind suspended water films at the mouths of the cavities underneath, which we refer to as 'capillary bridges'. (D) A zoomed image showing thin

films of water receding amidst capillary bridges. (E-F) A capillary bridge isolated from neighbors. We speculate that these bridges evaporate faster at the center than at boundaries and eventually break.

EXPERIMENTAL SECTION

The silicon wafers (4-inch diameter, <100> orientation and with 2.4 μm thick thermal oxide layer from Silicon Valley Microelectronics) were spin coated with a 1.6 μm layer of AZ-5214 photoresist. The patterns were designed using Tanner EDA L-Edit software and were transferred to the wafer in a Heidelberg Instruments μPG501 direct-writing system. The UV-exposed photoresist was removed in a bath of AZ-726 developer. The exposed SiO_2 top layer was etched away in an Inductively Coupled Plasma (ICP) Reactive-Ion Etching (RIE) equipment by Oxford Instruments (pressure of 10 mT, RF power at 100 W, ICP power at 1500 W, C_4F_8 at 40 sccm and O_2 at 5 sccm, at T = 10 °C, for 13 min). The wafer was then transferred to a Deep ICP-RIE (Oxford Instruments) to etch the Si under the SiO_2 layer. We used an anisotropic etching method characterized by a sidewall profile control using alternating deposition of a C_4F_8 passivation layer (pressure of 30 mT, RF at 5 W, ICP at 1300 W, C_4F_8 at 100 sccm and SF_6 at 5 sccm, at T = 15 °C for 5 s) and etching with SF_6 (pressure of 30 mT, RF at 30 W, ICP at 1300 W, C_4F_8 at 5 sccm and SF6 at 100 sccm, at T = 15 °C for 7 s). This process was cycled 4 times, which corresponds to an etching depth of ≈ 2 μm. After a piranha cleanse (H_2SO_4 : H_2O_2 :: 4:1) at T = 115 °C for 10 min a isotropic etching step was performed (pressure of 35 mT, RF at 20 W, ICP at 1800 W, SF_6 at 110 sccm, at T = 15 °C for 25 s). Then, a 300 nm layer of thermal oxide was grown over the etched wafer, using a Tystar furnace system. The top and bottom layers of thermal oxide were subsequently etched using the same recipe as in the first SiO_2 etching step. The next steps included a repetition of the 4 cycles of the anisotropic process used before, a piranha cleanse, followed by the isotropic step described earlier, to create the void behind the added sidewall of thermal oxide, which then formed the doubly reentrant rim at the edge of the cavity. The final step deepened the cavities up to ≈ 50 μm, using the same anisotropic recipe for 160 cycles. The samples were cleaned in piranha solution ($H_2SO_4 : H_2O_2$ :: 4:1) at T = 115 °C for 10 min), blown with N_2 pressure gun and thoroughly dried in an oven at 80 °C overnight. Subsequently, the samples were stored in plastic petri dishes till the intrinsic contact angle of smooth silica stabilized to, $\theta_o \approx 40°$. The static and advancing/receding contact angle measurement using de-ionized water and mineral oil (Light Mineral Oil, Fisher Scientific, CAS : 8042-47-5) were performed in a Kruss Drop Shape Analyzer - DSA100 at 0.2 μL s^{-1}. All the data were analyzed using the *Advance* software. Reported data points are an average of 5 to 10 measurements. Underwater and under mineral oil wetting transitions were observed using a Edmund Optics monochrome digital camera attached to Qioptics objective, with a focal distance of 9.5 cm. Selected samples were cleaved using diamond tip scribe and coated with a 4 nm Au/Pd layer before being observed by SEM (FEI Quanta 600). O_2 plasma cleaning was carried out in a Diener Electronics plasma system (Atto model), at power of 200 W for 10 min, using ultrapure (99.999%) O_2 gas supply with a flow 16.5 sccm. FDTS (perfluorodecyltrichlorosilane) deposition was performed using microprocessor controlled sequential depositor, ASMT Molecular Vapor deposition (MVD) 100E.

ASSOCIATED CONTENT

Supporting Information.

The following file is available free of charge.

Section S1, S2 and S3, refer to calculation of cavity dimensions and capillary lengths, application of Cassie-Baxter model and possible strategies to decrease contact angle hysteresis on surfaces with doubly reentrant cavities.

Table S1, Figures S1-S8 and Movies S1-S5 consolidate and support arguments made in the manuscript.

AUTHOR INFORMATION

Corresponding Author

* E-mail: himanshu.mishra@kaust.edu.sa

Present Addresses

Interfacial Lab, Water Desalination and Reuse Center, Biological and Environmental Science and Engineering, 4700 King Abdullah University of Science and Technology, 23955-6900 Thuwal, Kingdom of Saudi Arabia

Author Contributions

‡ E. M. D. and S. M. contributed equally to this work. HM wrote the manuscript and EMD and SM edited it. All authors have given approval to the final version of the manuscript.

Funding

The authors thank KAUST Baseline Research Funding (BAS/1/1070-01-01), Center Affiliated Fund (BAS/1/1070-01-03) and Start-up funds (BAS/1/1070-01-02).

Notes

The authors declare no competing financial interests.

ACKNOWLEDGMENTS

We thank Mr. Ulrich Buttner and Mr. Ahad A. Sayed from the KAUST Core Labs for their guidance in microfabrication. HM is thankful to Professor Jacob Israelachvili (University of California Santa Barbara) for introducing him to this subject, and Professors Jayanta Chakraborty (Indian Institute of Technology, Kharagpur) and Yair Kaufman (Ben-Gurion University, Israel) for scientific discussions. The authors thank Dr. Ivan Vakarelski and Professor Sigurdur Thoroddsen (KAUST) for providing silica surfaces with doubly reentrant pillars. We also acknowledge Mr. Ivan Gromicho, scientific illustrator at King Abdullah University of Science and Technology (KAUST) for preparing Figure 1 and Dr. Virginia Unkefer (KAUST) for assistance in editing the manuscript. Finally, the authors thank the Editor and the reviewers at ACS *Applied Materials & Interfaces* for constructive criticism.

REFERENCES

1. Bhushan, B.; Jung, Y. C.; Koch, K., Micro-, Nano- and Hierarchical Structures for Superhydrophobicity, Self-Cleaning and Low Adhesion. *Philos. T. R. Soc. A.* **2009,** *367* (1894), 1631-1672.
2. Wong, T. S.; Kang, S. H.; Tang, S. K. Y.; Smythe, E. J.; Hatton, B. D.; Grinthal, A.; Aizenberg, J., Bioinspired Self-Repairing Slippery Surfaces with Pressure-Stable Omniphobicity. *Nature* **2011,** *477* (7365), 443-447.
3. Golovin, K. K., S. P. R.; Lee, D. H.; DiLoreto, E. T.; Mabry, J. M.; Tuteja, A., Designing Durable Icephobic Surfaces. *Sci. Adv.* **2016,** *2* (e1501496).
4. Lee, J.; Laoui, T.; Karnik, R., Nanofluidic Transport Governed by the Liquid/Vapour Interface. *Nat. Nanotechnol.* **2014,** *9* (4), 317-323.
5. Lei, W. W.; Rigozzi, M. K.; McKenzie, D. R., The Physics of Confined Flow and its Application to Water Leaks, Water Permeation and Water Nanoflows: a Review. *Rep. Prog. Phys.* **2016,** *79* (2), 1-45.
6. Chen, J.; Razdan, N.; Field, T.; Liu, D. E.; Wolski, P.; Cao X.; Prausnitz J. M.; Radke, C. J., Recovery of Dilute Aqueous Butanol by Membrane Vapor Extraction with Dodecane or Mesitylene. *J. Membr. Sci.* **2017,** *528*, 103-111.
7. Xue, Z. X.; Cao, Y. Z.; Liu, N.; Feng, L.; Jiang, L., Special Wettable Materials for Oil/Water Separation. *J. Mater. Chem. A* **2014,** *2* (8), 2445-2460.
8. Zhang, L. B.; Zhong, Y. J.; Cha, D.; Wang, P., A Self-Cleaning Underwater Superoleophobic Mesh for Oil-Water Separation. *Sci. Rep-Uk* **2013,** *3*, 1-5.
9. Lee, C.; Choi, C.-H.; Kim, C.-J., Superhydrophobic Drag Reduction in Laminar Flows: a Critical Review. *Exp. Fluids* **2016,** *57* (176), 1-20.
10. Peichun, T.; Peters, A. M.; Pirat, C.; Wessling, M.; Lammertink, R. G. H.; Lohse, D., Quantifying Effective Slip Length over Micropatterned Hydrophobic Surfaces. *Phys. Fluids* **2009,** *21* (11), 1-8.
11. Golovin, K. B.; Gose, J.; Perlin, M.; Ceccio, S. L.; Tuteja, A., Bioinspired Surfaces for Turbulent Drag Reduction. *Philos. T. R. Soc. A.* **2016,** *374* (2073).
12. Lee, C.; Kim, C. J., Underwater Restoration and Retention of Gases on Superhydrophobic Surfaces for Drag Reduction. *Phys. Rev. Lett.* **2011,** *106* (1), 1-4.
13. Amabili, M.; Lisi, E.; Giacomello, A.; Casciola, C. M., Wetting and Cavitation Pathways on Nanodecorated Surfaces. *Soft Matter* **2016,** *12* (12), 3046-3055.
14. Leslie, D. C.; Waterhouse, A.; Berthet, J. B.; Valentin, T. M.; Watters, A. L.; Jain, A.; Kim, P.; Hatton, B. D.; Nedder, A.; Donovan, K.; Super, E. H.; Howell, C.; Johnson, C. P.; Vu, T. L.; Bolgen, D. E.; Rifai, S.; Hansen, A. R.; Aizenberg, M.; Super, M.; Aizenberg, J.; Ingber, D. E., A Bioinspired Omniphobic Surface Coating on Medical Devices Prevents Thrombosis and Biofouling. *Nat. Biotechnol.* **2014,** *32* (11), 1134-1140.
15. Cassie, A. B. D.; Baxter, S., Wettability of Porous Surfaces. *T. Faraday Soc.* **1944,** *40*, 546-550.
16. Wenzel, R. N., Resistance of Solid Surface to Wetting by Water. *Ind. Eng. Chem. Res.* **1936,** *28* (8), 988-984.
17. Ma, Z. Y.; Hong, Y.; Ma, L. Y.; Su, M., Superhydrophobic Membranes with Ordered Arrays of Nanospiked Microchannels for Water Desalination. *Langmuir* **2009,** *25* (10), 5446-5450.

18. Liu, K. S.; Yao, X.; Jiang, L., Recent Developments in Bio-Inspired Special Wettability. *Chem. Soc. Rev.* **2010,** *39* (8), 3240-3255
19. Neinhuis, C.; Barthlott, W., Characterization and Distribution of Water-Repellent, Self-Cleaning Plant Surfaces. *Ann. Bot-London* **1997,** *79* (6), 667-677.
20. Liu, K. S.; Tian, Y.; Jiang, L., Bio-inspired Superoleophobic and Smart Materials: Design, Fabrication, and Application. *Prog. Mater. Sci.* **2013,** *58* (4), 503-564.
21. Wong, T. S.; Sun, T. L.; Feng, L.; Aizenberg, J., Interfacial Materials with Special Wettability. *Mrs Bull.* **2013,** *38* (5), 366-371.
22. Nosonovsky, M.; Bhushan, B., Biologically inspired surfaces: Broadening the scope of roughness. *Adv. Funct. Mater.* **2008,** *18* (6), 843-855.
23. Tuteja, A.; Choi, W.; Mabry, J. M.; McKinley, G. H.; Cohen, R. E., Robust Omniphobic Surfaces. *P. Natl. Acad. Sci. U.S.A.* **2008,** *105* (47), 18200-18205.
24. Verho, T.; Bower, C.; Andrew, P.; Franssila, S.; Ikkala, O.; Ras, R. H. A., Mechanically Durable Superhydrophobic Surfaces. *Adv. Mater.* **2011,** *23*, 673-678.
25. Yang, F.; Zhu, L. Q.; Han, D. X.; Li, W. P.; Chen, Y. C.; Wang, X. M.; Ning, L., Preparation and Hydrophobicity Failure Behavior of Two Kinds of Fluorine-Containing Acrylic Polyurethane Coatings. *Rsc Advances* **2015,** *5* (115), 95230-95239.
26. Hendren, Z. D.; Brant, J.; Wiesner, M. R., Surface Modification of Nanostructured Ceramic Membranes for Direct Contact Membrane Distillation. *J. Membr. Sci.* **2009,** *331* (1-2), 1-10.
27. Metz, B.; al., e. *Safeguarding the Ozone Layer and the Global Climate System*; IPCC/TEAP: New York, **2005**.
28. Lindstrom, A. B.; Strynar, M. J.; Libelo, E. L., Polyfluorinated Compounds: Past, Present, and Future. *Environ. Sci. Technol.* **2011,** *45* (19), 7954-7961.
29. Herminghaus, S., Roughness-Induced non-Wetting. *Europhys. Lett.* **2000,** *52* (2), 165-170.
30. Abdelsalam, M. E.; Bartlett, P. N.; Kelf, T.; Baumberg, J., Wetting of Regularly Structured Gold Surfaces. *Langmuir* **2005,** *21* (5), 1753-1757.
31. Liu, J. L.; Feng, X. Q.; Wang, G. F.; Yu, S. W., Mechanisms of Superhydrophobicity on Hydrophilic Substrates. *J. Phys-Condens. Mat.* **2007,** *19* (35), 1-12.
32. Nosonovsky, M., Multiscale Roughness and Stability of Superhydrophobic Biomimetic Interfaces. *Langmuir* **2007,** *23* (6), 3157-3161.
33. Marmur, A., From Hygrophilic to Superhygrophobic: Theoretical Conditions for Making high-contact-angle Surfaces from low-contact-angle Materials. *Langmuir* **2008,** *24* (14), 7573-7579.
34. Hensel, R.; Helbig, R.; Aland, S.; Braun, H. G.; Voigt, A.; Neinhuis, C.; Werner, C., Wetting Resistance at Its Topographical Limit: The Benefit of Mushroom and Serif T Structures. *Langmuir* **2013,** *29* (4), 1100-1112.
35. Bormashenko, E., Progress in Understanding Wetting Transitions on Rough Surfaces. *Adv. Colloid. Interfac.* **2015,** *222*, 92-103.
36. Patankar, N. A., Thermodynamics of Trapping Gases for Underwater Superhydrophobicity. *Langmuir* **2016,** *32* (27), 7023-7028.
37. Hensel, R.; Finn, A.; Helbig, R.; Braun, H. G.; Neinhuis, C.; Fischer, W. J.; Werner, C., Biologically Inspired Omniphobic Surfaces by Reverse Imprint Lithography. *Adv. Mater.* **2014,** *26* (13), 2029-2033.

38. Hensel, R.; Neinhuis, C.; Werner, C., The Springtail Cuticle as a Blueprint for Omniphobic Surfaces. *Chem. Soc. Rev.* **2016,** *45* (2), 323-341.
39. Hensel, R.; Helbig, R.; Aland, S.; Voigt, A.; Neinhuis, C.; Werner, C., Tunable Nano-Replication to Explore the Omniphobic Characteristics of Springtail Skin. *Npg Asia. Mater.* **2013,** *5*, 1-6.
40. Liu, T. Y.; Kim, C. J., Turning a Surface Superrepellent even to Completely Wetting Liquids. *Science* **2014,** *346* (6213), 1096-1100.
41. Liu, T. Meniscus Shape Engineering Through Micro and Nano Fabrication. University of California Los Angeles, **2014**.
42. Butt, H.-J.; Kappl, M., *Surface and Interfacial Forces*. Wiley-VCH Verlag GmbH & Co.: Weinheim, **2010**.
43. Choi, W.; Tuteja, A.; Mabry, J. M.; Cohen, R. E.; McKinley, G. H., A Modified Cassie-Baxter Relationship to Explain Contact Angle Hysteresis and Anisotropy on non-Wetting Textured Surfaces. *J. Colloid. Interf. Sci.* **2009,** *339* (1), 208-216.
44. Liu, T. Y. L.; Chen, Z. Y.; Kim, C. J., A Dynamic Cassie-Baxter Model. *Soft Matter* **2015,** *11* (8), 1589-1596.
45. Chen, W.; Fadeev, A. Y.; Hsieh, M. C.; Oner, D.; Youngblood, J.; McCarthy, T. J., Ultrahydrophobic and Ultralyophobic Surfaces: Some Comments and Examples. *Langmuir* **1999,** *15* (10), 3395-3399.
46. Dufour, R.; Harnois, M.; Thomy, V.; Boukherroub, R.; Senez, V., Contact Angle Hysteresis Origins: Investigation on Super-Omniphobic Surfaces. *Soft Matter* **2011,** *7* (19), 9380-9387.
47. Yang, X. M.; Zhong, Z. W.; Diallo, E. M.; Wang, Z. H.; Yue, W. S., Silicon Wafer Wettability and Aging Behaviors: Impact on Gold Thin-Film Morphology. *Mat. Sci. Semicon. Proc.* **2014,** *26*, 25-32.
48. Habuka, H.; Ishiwari, S.; Kato, H.; Shimada, M.; Okuyama, K., Airborne Organic Contamination Bbehavior on Silicon Wafer Surface. *J. Electrochem. Soc.* **2003,** *150* (2), G148-G154.
49. Li, Z. T.; Wang, Y. J.; Kozbial, A.; Shenoy, G.; Zhou, F.; McGinley, R.; Ireland, P.; Morganstein, B.; Kunkel, A.; Surwade, S. P.; Li, L.; Liu, H. T., Effect of Airborne Contaminants on the Wettability of Supported Graphene and Graphite. *Nat. Mater.* **2013,** *12* (10), 925-931.
50. Philip, J. R., Kinetics of Capillary Condensation in Wedge-Shaped Pores. *J. Chem. Phys.* **1964,** *41* (4), 911-916.
51. Dong, M.; Chatzis, I., The Imbibition and Flow of a Wetting Liquid along the Corners of a Square Capillary Tube. *J. Colloid. Interf. Sci.* **1995,** *172*, 278-288.
52. Ransohoff, T. C.; Radke, C. J., Laminar-Flow of a Wetting Liquid Along the Corners of a Predominantly Gas-Occupied Noncircular Pore. *J. Colloid. Interf. Sci.* **1988,** *121* (2), 392-401.
53. Kim, E.; Whitesides, G. M., Imbibition and Flow of Wetting Liquids in Noncircular Capillaries. *J. Phys. Chem. B* **1997,** *101* (6), 855-863.
54. Liu, Y. H.; Nolte, D. D.; Pyrak-Nolte, L. J., Pinned Films and Capillary Hysteresis in Microfluidic Channels. *Lab. Chip.* **2012,** *12* (16), 2858-2864.
55. Penas-Lopez, P.; Parrales, M. A.; Rodriguez-Rodriguez, J., Dissolution of a CO2 Spherical Cap Bubble Adhered to a Flat Surface in Air-Saturated Water. *J. Fluid Mech.* **2015,** *775*, 53-76.
56. de Gennes, P.-G., Brodchard-Wyart, F., Quere, D., *Capillarity and Wetting Phenomena: Drops, Bubbles, Pearls, Waves*. Springer; 2004 edition: **2003**.

57. Adamson, A. W., Gast, A. P., *Physical Chemistry of Surfaces*. Wiley-Interscience: Weinheim, **1997**.
58. Bonn, D.; Eggers, J.; Indekeu, J.; Meunier, J.; Rolley, E., Wetting and Spreading. *Rev. Mod. Phys.* **2009,** *81* (2), 739-805.
59. Lafuma, A.; Quere, D., Superhydrophobic States. *Nat. Mater.* **2003,** *2* (7), 457-460.
60. Mishra, H.; Schrader, A. M.; Lee, D. W.; Gallo, A.; Chen, S. Y.; Kaufman, Y.; Das, S.; Israelachvili, J. N., Time-Dependent Wetting Behavior of PDMS Surfaces with Bioinspired, Hierarchical Structures. *Acs Appl. Mater. Inter.* **2016,** *8* (12), 8168-8174.
61. Kaufman, Y.; Chen, S.-Y.; Mishra, H.; Schrader, A. M.; Lee, D. W.; Das, S.; Donaldson, S. H.; Israelachvili, J. N., A Simple to Apply Wetting Model to Predict Thermodynamically Stable and Metastable Contact Angles On Textured/Rough/Patterned Surfaces. *J. Phys. Chem. C* **2017,** *121* (10), 5642-5656.
62. Patankar, N. A., Hydrophobicity of Surfaces with Cavities: Making Hydrophobic Substrates from Hydrophilic Materials? *J. Adhes. Sci. Technol.* **2009,** *23* (3), 413-433.
63. Xu, M. C.; Sun, G. U.; Kim, C. J., Infinite Lifetime of Underwater Superhydrophobic States. *Phys. Rev. Lett.* **2014,** *113* (13), 1-5.
64. Jones, P. R.; Hao, X.; Cruz-Chu, E. R.; Rykaczewski, K.; Nandy, K.; Schutzius, T. M.; Varanasi, K. K.; Megaridis, C. M.; Walther, J. H.; Koumoutsakos, P.; Espinosa, H. D.; Patankar, N. A., Sustaining Dry Surfaces Under Water. *Sci. Rep-Uk* **2015,** *5*, 1-10.
65. Epstein, P. S.; Plesset, M. S., On the Stability of Gas Bubbles in Liquid-Gas Solutions. *J. Chem. Phys.* **1950,** *18* (11), 1505-1509.
66. Lv, P. Y.; Xue, Y. H.; Liu, H.; Shi, Y. P.; Xi, P.; Lin, H.; Duan, H. L., Symmetric and Asymmetric Meniscus Collapse in Wetting Transition on Submerged Structured Surfaces. *Langmuir* **2015,** *31* (4), 1248-1254.
67. Xiang, Y. L.; Xue, Y. H.; Lv, P. Y.; Li, D. D.; Duan, H. L., Influence of Fluid Flow on the Stability and Wetting Transition of Submerged Superhydrophobic Surfaces. *Soft Matter* **2016,** *12* (18), 4241-4246.
68. Heshmati, M.; Piri, M., Experimental Investigation of Dynamic Contact Angle and Capillary Rise in Tubes with Circular and Noncircular Cross Sections. *Langmuir* **2014,** *30* (47), 14151-14162.
69. Mielonen, K.; Suvanto, M.; Pakkanen, T. A., Curved Hierarchically Micro-Micro Structured Polypropylene Surfaces by Injection Molding. *J. Micromech. Microeng.* **2017,** *27* (1), 1-10.

Table of Contents Schematic: